

## Three-Component Porous–Carbon–Titania Nanocomposites through Self-Assembly of ABCBA Block Terpolymers with Titania Sols

Morgan Stefik,<sup>†</sup> Hiroaki Sai,<sup>†</sup> Kenneth Sauer,<sup>‡</sup> Sol M. Gruner,<sup>§,||</sup> Francis J. DiSalvo,<sup>⊥</sup> and Ulrich Wiesner<sup>\*†</sup>

<sup>†</sup>Department of Materials Science and Engineering, Cornell University, Ithaca, New York 14853, <sup>‡</sup>Department of Environmental Engineering, Cornell University, Ithaca, New York 14853, <sup>§</sup>Department of Physics, Cornell University, Ithaca, New York 14853, <sup>||</sup>Cornell High Energy Synchrotron Source, Cornell University, Ithaca, New York 14853, and <sup>⊥</sup>Department of Chemistry and Chemical Biology, Cornell University, Ithaca, New York 14853

Received March 31, 2009; Revised Manuscript Received July 2, 2009

**ABSTRACT:** We report the first use of a block terpolymer for the synthesis of three-component nanocomposites. Here, the use of three chemically distinct polymer blocks enabled control over each of the three final components: partially graphitic carbon, crystalline transition metal oxide, and porosity. Tuning of the individual block lengths and block fractions resulted in control over the three components. Specifically, two PAN-*b*-PEO-*b*-PPO-*b*-PEO-*b*-PAN pentablock terpolymers were synthesized starting with a functionalized P123 or F127 macroinitiator. The PEO blocks were selectively swelled with titania sols while the PPO primarily served as a mesoporosity source and the PAN served as a carbon source with high yield. Two subsequent heat treatments were used to form partially graphitic carbon which acted as an in situ hard template preserving the mesostructure through the crystallization of the titania sols. TEM and SAXS analysis revealed wormlike microphase separation. Nitrogen physisorption analysis revealed that the pore size distributions for all nanocomposites were narrow and the distribution centers were tuned from 6.0 to 16.5 nm. The carbon content of the nanocomposites was varied from 11.3 to 35.2 wt % by increasing the fraction of PAN in the hybrids.

### Introduction

The self-assembly of amphiphilic block copolymers has been extensively applied toward the structure-directing of porous materials. Generally, the hydrophilic block is selectively swelled with hydrophilic nanoparticles or molecular precursors via van der Waals or ionic interactions while the hydrophobic block repels these precursors.<sup>1</sup> Subsequent pyrolysis of such composites generates porous materials by removal of the polymer. This or similar approaches have been broadly applied to generate mesoporous silicates,<sup>2</sup> aluminosilicates,<sup>3</sup> transition metal oxides,<sup>4–7</sup> platinum,<sup>8</sup> and carbon<sup>9–13</sup> materials. Most examples of block copolymer derived porous multimaterial composites were synthesized by selectively swelling the hydrophilic block of a block copolymer with a mixture of multiple hydrophilic precursors which resulted in a random dispersion of the two materials with ordered pores.<sup>14–16</sup> In order to structure-direct multiple materials separately, other approaches have utilized block copolymers where the hydrophobic block served as a carbon source to form silica–carbon<sup>17</sup> or titania–carbon<sup>18</sup> nanocomposites. The recently published CASH method utilized hydrophobic poly(isoprene) as both a porosity source and a carbon source to enable the preservation of the mesostructure during the high-temperature crystallization of the transition metal oxides.<sup>19</sup> While this approach resulted in porous transition metal oxides with a small amount of carbon, it did not demonstrate direct control over the amount of carbon. Many of these approaches may be combined conceptually by utilizing an amphiphilic block terpolymer (having three chemically different mer units) with, for example, two different hydrophobic blocks—one hydrophobic block generates porosity, the other hydrophobic block generates carbon in high yield, and the

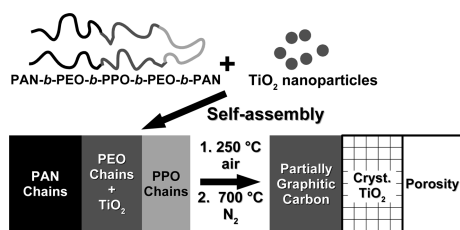
hydrophilic block selectively swells with sol particles. Such a method would enable block sequence directed materials (BSDMs), where a sequence of three or more chemically different polymer blocks directs the spatial arrangement and interface definitions of multiple functional materials. The achievement of BSDMs would be a significant step toward mimicking the more complex assembly processes that result in biological nanocomposites. While there have been a few papers on aluminosilicate structure-directing with block terpolymers,<sup>20,21</sup> there are no reports, to the best of our knowledge, that have utilized a block terpolymer to synthesize three-component nanocomposites.

Nanocomposite materials have attracted considerable attention due to their often novel properties. Such nanocomposites are not only more homogeneous than their bulk analogues but sometimes also enable new functionality.<sup>22,23</sup> For example, bulk titania has poor electrode performance in Li-ion battery applications due to its very low Li diffusivity and poor electrical conductivity (semiconductor). However, porous nanoscale composites of titania with good electrical conductors, such as carbon, enable the use of titania for Li-ion battery anodes. Furthermore, shrinking the Li diffusion length in titania enables utilization of titania's fast Li insertion/desertion kinetics.<sup>24,25</sup> Similarly, such porous–oxide–carbon nanocomposites could also function as fuel cell electrodes by utilizing the surface proton conductivity of oxides which is comparable to that of Nafion.<sup>26,27</sup> Three-component nanocomposites are of great general interest for electrochemical devices such as batteries and fuel cells which all require multiple continuous pathways for the reaction of (1) reducing/oxidizing species with (2) electrons and (3) ions.<sup>28</sup>

Here we report on the one-pot synthesis of three-component nanocomposites directly from the self-assembly of block terpolymers with transition metal oxide sols. Specifically, the PEO blocks of PAN-*b*-PEO-*b*-PPO-*b*-PEO-*b*-PAN pentablock terpolymers

\*To whom correspondence should be addressed. E-mail: ubw1@cornell.edu.

**Scheme 1. Schematic Representation of “One-Pot” Synthesis of Mesoporous Porous/Carbon/Titania Nanocomposites via Self-Assembly of a Pentablock Terpolymer with TiO<sub>2</sub> Sols Followed by Specific Heat Treatments**



were selectively swelled with titania sols. Subsequent heat treatments transformed the microphase-separated materials into mesoporous—partially graphitic carbon—anatase titania nanocomposites (Scheme 1). A nanocomposite was also made using as-received P123 for comparison. Tuning of the individual block lengths and block fractions resulted in control of all three components in three different samples: Cornell composition of materials with pores, carbon, and titania (CCM-PCT-1, CCM-PCT-2, and CCM-PCT-3).

## Experimental Section

**Materials and Instrumentation.** *Materials.* For the macroinitiator synthesis, 2-bromo-2-methylpropionic acid (98%, BiB), *N,N'*-dicyclohexylcarbodiimide (99%, DCC), 4-(dimethylamino)pyridine (99%, DMAP), poly(ethylene oxide)-*block*-poly(propylene oxide)-*block*-poly(ethylene oxide) triblock copolymers Pluronic P123 (PEO<sub>20</sub>PPO<sub>70</sub>PEO<sub>20</sub>) and F127 (PEO<sub>106</sub>-PPO<sub>70</sub>PEO<sub>106</sub>), and anhydrous, methanol-free chloroform (99%) were purchased from Sigma-Aldrich and used as received.

For the PAN chain extension, acrylonitrile (99%, AN), CuBr (99.999%), CuBr<sub>2</sub> (99.999%), basic alumina (activity I, MP Biomedical), 1,1,4,7,10,10-hexamethyltriethylenetetramine (97%, HMTETA), *N,N*-dimethylformamide (99.9%, DMF), and ethylene carbonate (99%, EC) were purchased from Sigma-Aldrich and used as received. SnakeSkin dialysis tubing with a 3.5 kg/mol molecular weight cutoff was purchased from Pierce. Deionized water was prepared from a Barnstead NANOpure filtration system.

For the composite synthesis, titanium(IV) chloride (99%, Sigma-Aldrich), titanium(IV) isopropoxide (97%, Sigma-Aldrich), 37 wt % hydrochloric acid (ACS grade, BDH), NaBr (99%, Sigma-Aldrich), and anhydrous ethanol (99%, Pharmco) were used as received. DMF and deionized water were used for composite synthesis as detailed above.

*Instrumentation.* *Gel permeation chromatography (GPC)* measurements were performed in DMF with 10 μm Polymer Standards Service (PSS, Warmick, RI) GRAM columns (10<sup>2</sup>, 10<sup>3</sup>, 3 × 10<sup>3</sup> Å, 300 mm long each, and 8 mm in diameter) at a flow rate of 1.0 mL/min. An Agilent 1200 refractive index detector operated at 40 °C was used to detect the polymer. Raw data were processed using PSS-Win GPC V6.2 software. Molecular weight distributions ( $M_w/M_n$ ) were calculated using a poly(styrene) calibration curve.

*<sup>1</sup>H Nuclear Magnetic Resonance (NMR).* <sup>1</sup>H solution NMR spectra were recorded on a Varian INOVA 400 MHz spectrometer using the deuterated chloroform signal ( $\delta = 7.27$  ppm) or the deuterated dimethyl sulfoxide signal ( $\delta = 2.50$  ppm) as an internal standard.

*Transmission Electron Microscopy (TEM).* Samples were ultrathin sectioned at -55 °C with a Leica Ultracut UCT microtome. Sample slices were collected on a water/DMSO eutectic solution and transferred to 300 mesh copper grids (no carbon film). A Technai T12 operating at 120 kV was used to image the sections.

*Small-Angle X-ray Scattering (SAXS).* SAXS data were collected on a Rigaku RU300 which used a copper rotating anode ( $\lambda = 1.54$  Å) operated at 40 kV and 50 mA. The X-rays were monochromated using a Ni filter and focused using orthogonal Franks mirrors. The SAXS patterns were collected with a home-built 1K × 1K pixel CCD detector similar to that described elsewhere.<sup>29</sup> Data are presented as  $q = 4\pi \sin(\theta)\lambda^{-1}$ , where  $2\theta$  is the total scattering angle.

*Raman Spectroscopy.* Raman spectra were collected on a Renishaw InVia microRaman system using a 488 nm laser.

*Powder X-ray diffraction (XRD).* XRD spectra were collected on a Scintag  $\theta$ - $\theta$  diffractometer using Cu K $\alpha$  radiation ( $\lambda = 1.54$  Å).

*Thermal Gravimetric Analysis (TGA).* TGA analysis was performed with flowing air on a TG/DTA 320 at a heating rate of 20 °C/min to 550 °C and held for 2 h. The sample mass in all TGA curves was normalized at 150 °C to eliminate mass loss due to water desorption.

*Nitrogen Physisorption Analysis.* Isotherms were measured at -196 °C using a Micromeritics ASAP 2020 system. The samples were degassed at 150 °C overnight under high vacuum. The Brunauer, Emmett, and Teller (BET) and Brunauer, Jonyer, and Halenda (BJH) analyses were performed using Micromeritics ASAP 2020 V1.05 software.

**Synthesis.** *Macroinitiator Synthesis.* The P123- and F127-based macroinitiators were both prepared in a similar fashion to that reported previously.<sup>30</sup> The diol Pluronic triblock copolymer was dried at 40 °C under high vacuum to remove trace water. The Pluronic polymer was then dissolved in dry, methanol-free chloroform to form a 30 wt % polymer solution under constant stirring. Then, BiB was added to the solution in a 2.35:1 molar ratio of BiB:polymer with an overflow of nitrogen. The solution was cooled in an ice bath before the next additions. Then, DCC was added to the stirred solution and quickly followed by DMAP in a 2.35:0.37:1 molar ratio of DCC:DMAP:polymer. The solution turned cloudy indicating transformation of the DCC to the corresponding urea. The reaction was stirred for 5 min in contact with the ice bath and then allowed to stir at room temperature for 1 day. The polymer solution was filtered through a glass frit to remove most of the urea and then syringe filtered. The chloroform was removed with rotary evaporation, and the polymer was redissolved in THF and refiltered. The THF was then removed by rotary evaporation and the product was dried under high vacuum for at least 1 day. <sup>1</sup>H NMR spectroscopy was used to confirm the quantitative chain end transformation of the Pluronic polymer to form the macroinitiator (Pluronic-Br<sub>2</sub>) with a bromine end group at each end (Supporting Information Figure S1A).

*PAN Chain Extension.* Acrylonitrile was flowed over basic alumina to remove the inhibitor. Each polymerization was carried out in a glass reactor equipped with a septum and attached to a Schlenk line via a rubber hose. The Pluronic-Br<sub>2</sub> macroinitiator was added to reactor along with a stir bar. Nitrogen was flowed through the reactor as molten EC and AN were added via the septum port. The reactor contents were stirred at 40 °C until a homogeneous solution was formed. The septum was replaced, and the reactor was subjected to three freeze-pump-thaw cycles and then backfilled with positive nitrogen pressure. Two catalyst stock solutions were prepared separately in a glovebox. The CuBr stock solution contained equal moles of CuBr and degassed HMTETA and was dissolved in degassed DMF to a concentration of 10 mg of CuBr per mL. The CuBr<sub>2</sub> solution was prepared in the same fashion. The reactor was placed in an oil bath maintained at 55 °C by a stirring hot plate. The CuBr<sub>2</sub> stock solution was added to the reactor via the septum, followed by the CuBr stock solution. All polymerizations were carried out with molar ratios of 0.5:0.1:0.08:0.02:250 for Pluronic-Br<sub>2</sub>:HMTETA:CuBr:CuBr<sub>2</sub>:AN with EC added to make the initial AN concentration 5.25 M. A timer was started immediately, and the polymerization was stopped at the desired conversion by exposing the

reactor contents to air. The reaction contents were diluted to twice the volume with DMF and dialyzed against deionized water three times for at least 12 h. The contents of the dialysis bag were rotary evaporated to remove water and then dried for a day under high vacuum. The resulting product was white to yellow depending on the amount of PAN grown. The resulting PAN-*b*-PEO-*b*-PPO-PEO-*b*-PAN pentablock terpolymer (Pluronic-PAN) was characterized by  $^1\text{H}$  NMR and GPC. The PAN molecular weight was calculated from the  $^1\text{H}$  NMR data, and the polydispersity was determined by GPC (Supporting Information Figures S1B–D). Two different terpolymers were used to make nanocomposites: Pluronic-PAN1 and Pluronic-PAN2. Pentablock terpolymer Pluronic-PAN1 was synthesized from P123, had a number-average molecular weight of 6.35 kg/mol and a polydispersity of 1.52, and was composed of 8.25 wt % PAN and 27.7 wt % PEO. Pluronic-PAN2 was synthesized from F127, had a number-average molecular weight of 21.5 kg/mol and a polydispersity of 1.37, and was composed of 37.7 wt % PAN and 43.4 wt % PEO. The as-received P123 and F127 had reported number-average molecular weights of 5.8 and 12.6 kg/mol, respectively. The polydispersities of P123 and F127 were determined with GPC to be 1.34 and 1.46, respectively (Figures S1C,D). For nanocomposite comparison, a third sample was synthesized using as-received P123. All polymers used had a 4.1 kg/mol PPO center block.

**Composite Synthesis.** All composites were synthesized using hydrolytic sol–gel routes for titania. Each sample was synthesized from a different polymer. CCM-PCT-1 was synthesized by dissolving 0.109 g of Pluronic-PAN1 in 3.7 mL of ethanol and 0.3 g of hydrochloric acid under rapid stirring at 85 °C for 3 h. The solution was cooled to 40 °C, and 0.313 mL of titanium isopropoxide was added while stirring. The solution was stirred at 40 °C for 20 h. The solution was cast in a Teflon dish inside a box oven set to 35 °C with 50–60% RH maintained by a stirred and fan-blown saturated aqueous NaBr salt bath for 5 days. The film was then heated to 80 °C for 7 more days to cross-link the sol. The film was then heated in air at 1 °C/min to 250 °C and held for 2 h to cyclize the PAN. Lastly, the film was heated at 1 °C/min to 700 °C under nitrogen flow and held for 2 h to carbonize the PAN and crystallize the titania.

CCM-PCT-2 was synthesized by dissolving 0.250 g of Pluronic-PAN2 in 25 mL of DMF followed by the dropwise addition of 0.91 mL of ethanol. The polymer solution was brought into a glovebag where 0.171 mL of titanium chloride was added under rapid stirring. The solution was stirred for an hour before being cast in an open Teflon dish maintained at 40 °C for 7 days. The film was dried under high vacuum for several hours and then subjected to the same 250 and 700 °C heat treatments under air and nitrogen, respectively.

For comparison, sample CCM-PCT-3 was synthesized from as-received P123. The same conditions were used as previously reported by the Zhao group for pure  $\text{TiO}_2$ ,<sup>31</sup> except the calcination steps were performed using the same two step heat treatment used for samples CCM-PCT-1 and CCM-PCT-2.

## Results and Discussion

**1. Synthesis of Pluronic-PAN Pentablock Terpolymers.** Pluronic block copolymers P123 and F127 have been extensively studied for structure-directing porous materials and thus serve as a suitable starting point for block terpolymer synthesis. We sought to add graphitic carbon to these nanocomposites to aim for the high electrical conductivity and thermodynamic stability desirable for electron conduction in electrochemical applications. Poly(acrylonitrile) is a well-established source of graphitic carbon and is commercially used for the production of graphitic carbon fibers.<sup>32</sup> There are numerous examples of the controlled radical polymerization of PAN, especially using atom transfer radical polymerization (ATRP).<sup>17,33–40</sup> To this end, an initiator

of suitable kinetic activity<sup>41</sup> for PAN growth was attached to the alcohol end groups of Pluronic block copolymers via a Steglich esterification. The resulting Pluronic-Br<sub>2</sub> macroinitiator was then used for chain extension using ATRP. ATRP of PAN can be challenging due to a side reaction with the activator CuBr, often limiting achievable molecular weights to ca. 10 kg/mol.<sup>35</sup> Although AGET ATRP was shown to greatly suppress this side reaction,<sup>39</sup> standard ATRP was instead used to keep the polydispersity as low as possible. To this end, all polymerizations were performed with a 10:0.8 ratio of chain ends to CuBr. This side reaction was further suppressed by utilizing a tetradentate ligand (HMTETA) to saturate the coordination sites of the Cu better than the commonly employed bipyridine ligands. HMTETA has a similar kinetic activity to bipyridine<sup>42</sup> and was found (unpublished work) to enable the synthesis of much larger PAN blocks with similarly low polydispersities. The purified product was characterized by NMR to determine the PAN molecular weight and GPC to determine the polydispersity. The GPC elugrams of the starting triblock copolymers P123 and F127 had bimodal molecular weight distributions as previously reported.<sup>43</sup> Elugrams of Pluronic-PAN1 and Pluronic-PAN2 showed a shift to higher molecular weights while maintaining similar polydispersities to the parent Pluronic polymers (Figures S1C,D).

**2. Synthesis of Mesoporous–Carbon–Titania Nanocomposites.** A simple “one-pot” approach was used to synthesize three-component nanocomposites. The structure-directing polymer was dissolved in a suitable solvent, and a hydrolytic titania sol was synthesized in the same solution. Films were cast to remove volatile solvents, leading to microphase separation of polymer blocks with the titania sol particles selectively swelling the hydrophilic PEO block. The titania sol is highly protonated under the acidic conditions typically utilized and does not condense appreciable until sufficient HCl has volatilized.<sup>6</sup> The films were aged at a low temperature to provide time for titania gelation before further heat treatments. The subsequent heat treatment to 250 °C in air is well-known to cyclize the PAN blocks to form a rigid-ladder-like polymer backbone which increases the carbon yield. The cyclized PAN chains further react thermally in inert atmosphere via dehydrogenation (400–600 °C) and denitrogenation (600–1300 °C) reactions to form carbon materials.<sup>32</sup> The second heat treatment to 700 °C under nitrogen carbonized the PAN, crystallized the amorphous titania sol, and generated mesoporosity from the PPO pyrolysis.

The microphase separation of Pluronic-PAN and as-cast nanocomposites was investigated with diffraction studies. The XRD spectrum of neat Pluronic-PAN2 has peaks at 17.0°, 19.2°, and 23.3° (Figure 1D, bottom). The peaks at 19.2° and 23.3° correspond to PEO crystallites,<sup>44</sup> and the peak at 17.0° corresponds to PAN crystallites.<sup>45</sup> The XRD observation of separate PEO and PAN crystallites is consistent with the expected microphase separation of the semicrystalline PEO, semicrystalline PAN, and amorphous PPO domains. Furthermore, the SAXS patterns of Pluronic-PAN1 and Pluronic-PAN2 each have a single broad peak at ca. 11 and 15 nm, respectively, corresponding to the short-range order resulting from wormlike microphase separation of the neat polymers. These results were not unexpected considering that both PEO-*b*-PPO-*b*-PEO<sup>43</sup> and PEO-*b*-PAN<sup>17</sup> polymers are known to microphase separate. The composite materials resulting from Pluronic-PAN polymers had similar XRD peaks at 17.0°, 19.2°, and 23.3° in addition to a broad peak centered near 25° (Figure 1D, top). The presence of PAN and PEO crystallites in composite materials is again a strong indication for the microphase separation of

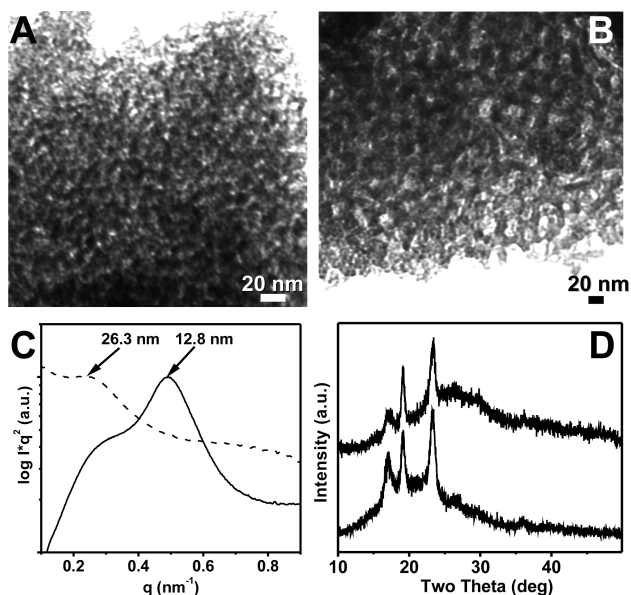


**Figure 1.** TEM images of three-component porous-carbon-titania nanocomposites CCM-PCT-1 (A) and CCM-PCT-2 (B) with wormlike structures resulted from microphase separation of Pluronic-PAN1 and Pluronic-PAN2 block terpolymers, respectively. SAXS (C) of CCM-PCT-1 (solid line) and CCM-PCT-2 (dashed line) nanocomposites exhibited a single peak corresponding to the length scale of the microphase separation. XRD (D) of neat Pluronic-PAN (bottom) and an as-cast film CCM-PCT-2 (top) show discrete crystallites of PAN and PEO indicating block terpolymer microphase separation before pyrolysis.

PAN, PEO, and PPO. The broad peak centered near  $25^\circ$  is attributed to the amorphous titania sol. Although PEO crystallization is known to be suppressed by the fractal oxide networks resulting from silicate sol-gel processes,<sup>3</sup> the close oxide particles<sup>6</sup> resulting from the hydrolytic titania sol-gel processes used here did not completely suppress the PEO crystallization. The complete mixing of PEO with oxide sol particles, and thus complete suppression of PEO crystallization, is not necessary for PEO-based amphiphiles to structure-direct oxide materials.<sup>46</sup> We suspect that the titania sol is mixed selectively with the amorphous regions of the PEO<sup>47</sup> and excluded from the crystalline PEO regions. Although mechanistically interesting, the small regions of crystalline PEO did not prevent the synthesis of three-component nanocomposites.

We take the three-component nanocomposite CCM-PCT-1 as a representative example of composites synthesized from Pluronic-PAN block terpolymers. The bright field TEM image of the final calcined porous-carbon-titania nanocomposite (Figure 1A) showed wormlike phase separation of the porosity (light) from the carbon and titania (both dark) with a period of ca. 13 nm. Contrast was not observed between the carbon and titania components in bright field TEM. Such short-range ordered microphase separation is commonly found in mesostructures derived from PAN based block copolymers<sup>38,48–52</sup> due to the high glass transition temperature (85–110 °C) and high melting temperature (320 °C) for the partially crystalline PAN block.<sup>53</sup> The single SAXS peak at 12.8 nm was consistent with the observed length scale of the wormlike morphology in TEM.

The titania and carbon of CCM-PCT-1 were further characterized to determine their type and relative proportions. The XRD spectrum showed several well-resolved peaks on a flat baseline, suggesting that the amorphous titania sol particles were successfully converted to crystalline material (Figure 2A). All of the observed XRD peaks were

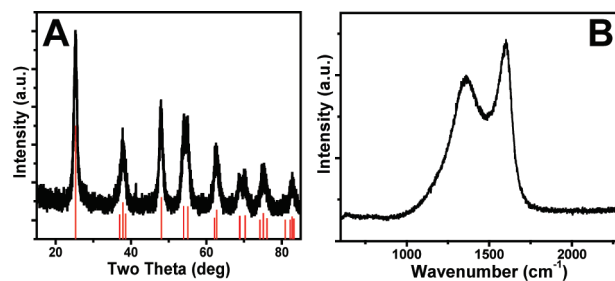


**Figure 2.** Powder XRD of CCM-PCT-1 (A) matches the indicated peaks for anatase titania (PDF #21-1272). The Raman spectrum of CCM-PCT-1 (B) was consistent with partially graphitic carbon.

consistent with the anatase phase of titania (PDF no. 21-1272). The Debye-Scherrer formula was used to calculate the crystallite size from the peak widths. This equation was applied to the nonoverlapping peaks near  $25^\circ$  and  $48^\circ 2\theta$  to calculate an average crystallite size of 9.4 nm. The titania crystallite size was consistent with length scale of the microphase separation determined by TEM (13 nm) and SAXS (12.8 nm). Furthermore, dark field TEM was used to directly view the 9–14 nm diameter titania nanoparticles (Figure S4). Raman spectroscopy was used to determine the type of carbon in the nanocomposite. The Raman spectrum had two pronounced peaks centered at 1600 and 1358  $\text{cm}^{-1}$ , respectively. Often, Raman spectra of carbon materials are convolutions of several peaks, possibly including those for ideal graphite (G 1580  $\text{cm}^{-1}$ ), a disordered graphitic lattice (D1 1350  $\text{cm}^{-1}$ , D2 1620  $\text{cm}^{-1}$ , and D4 1200  $\text{cm}^{-1}$ ), or amorphous carbon (D3 1500  $\text{cm}^{-1}$ ).<sup>54</sup> The significant G, D1, and D2 character in the Raman spectrum of CCM-PCT-1 was consistent with partially graphitic carbon composed of turbostratic graphite crystallites less than 7 nm in extent and with very little amorphous content (D3).<sup>55,56</sup> Partially graphitic carbon is expected to result from such a low carbonization temperature. The fraction of carbon in the nanocomposite was determined by oxidative TGA (Figure 3A, solid line). The sample had a single mass loss step starting at ca. 400 °C corresponding to oxidative removal of the carbon from the nanocomposite. CCM-PCT-1 lost 13.9% of the normalized mass, suggesting that the composite was composed of 13.9 wt % carbon. The change in sample color from black initially to white after TGA further supports that the mass loss is due to the loss of carbon. The amount of carbon in the nanocomposite is consistent with the typical 50 wt % carbon yield for PAN<sup>32</sup> combined with a ca. 10 wt % carbon yield for the Pluronic (discussed further for CCM-PCT-3). The XRD, Raman, and TGA data suggest that CCM-PCT-1 was composed of crystalline anatase titania and 13.9 wt % partially graphitic carbon.

A nitrogen physisorption experiment was performed to characterize the porosity in CCM-PCT-1. The nanocomposite had a type IV isotherm (Figure 3B, solid line), indicating that it had open and accessible mesoporosity. Our previously published work utilizing PEO-*b*-PAN structure-directing agents<sup>18</sup> were not mesoporous, indicating the need for an additional hydrophobic block as a mesoporosity source. A narrow pore size distribution centered at 10.0 nm was calculated from the adsorption branch of the isotherm using the BJH model (Figure 3B inset, solid line). The average mesopore size of CCM-PCT-1 was considerably larger than the 5–9 nm pore sizes normally resulting from the microphase separation of P123-based hybrids.<sup>2</sup> We suspect that the crystallization of the PAN stretches the PEO and PPO blocks, an effect thoroughly investigated in a recent study.<sup>57</sup> Such a stretched conformation of the PPO is consistent with

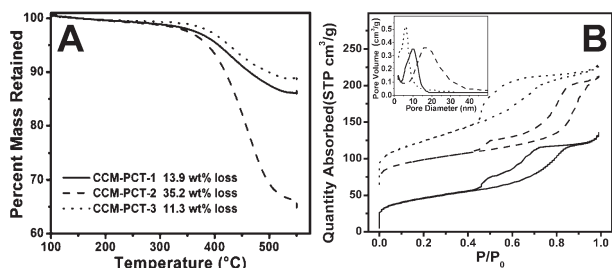


**Figure 3.** Oxidative TGA (A) was used to determine the carbon content of each nanocomposite. Nitrogen physisorption isotherms (B) were used to calculate the mesoporous surface area, microporous surface area, pore volume, and pore size distribution (inset) for each nanocomposite. Isotherms were offset to aid viewing. Tuning of the terpolymer block lengths enabled control over the porosity and carbon content of the nanocomposites.

the increased pore size. Sample CCM-PCT-1 had  $0.21 \text{ cm}^3/\text{g}$  of pore volume, and the BET model was used to determine that the nanocomposite had a total surface area of  $163 \text{ m}^2/\text{g}$ . The sample had  $36 \text{ m}^2/\text{g}$  of microporous surface area primarily due to the presence of carbon. Subtraction of the microporous surface area from the total surface area revealed that CCM-PCT-1 had  $127 \text{ m}^2/\text{g}$  of mesoporous surface area. The physisorption analysis revealed that nanocomposite CCM-PCT-1 had both mesoporosity and microporosity consistent with the microphase separation and carbon yield of the block terpolymer used.

Sample CCM-PCT-1, to the best of our knowledge, is the first three-component nanocomposite synthesized directly from the microphase separation of a block terpolymer. The use of a simple “one-pot” approach enabled the synthesis of a mesoporous nanocomposite composed of partially graphitic carbon and crystalline anatase titania.

**3. Composition and Porosity Control with Polymer Variation.** A different nanocomposite, CCM-PCT-2, was synthesized from Pluronic-PAN2 for comparison. The polymer used in this case was based instead on F127 which has the same PPO center but longer PEO blocks. Furthermore, in this case much longer PAN blocks were grown from the ends of the macroinitiator. Bright field TEM of the final calcined three-component nanocomposite again showed wormlike phase separation of the block terpolymer (Figure 1B). The 29 nm worm spacing was larger than in CCM-PCT-1 (13 nm), which was consistent with the longer block terpolymer used for CCM-PCT-2. The increased length scale of the microphase separation was further supported by the shift of the SAXS peak to a lower  $q$  value, corresponding to 26.3 nm (Figure 1C). The XRD and Raman spectroscopy were again consistent with crystalline anatase titania (average domain size 9.4 nm) and partially graphitic carbon. The TEM, SAXS, XRD, and Raman spectroscopy of CCM-PCT-2 were qualitatively similar to CCM-PCT-1, except the phase separation occurred on a longer length scale consistent with the longer block terpolymer used.

The differences in carbon content and porosity were characterized by TGA and nitrogen physisorption analysis. The oxidative TGA of CCM-PCT-2 exhibited a single weight loss step starting around  $400 \text{ }^\circ\text{C}$ , suggesting that this nanocomposite contained 35.2 wt % carbon (Figure 3A, dashed line). The carbon content was again consistent with the expected 50 wt % carbon yield from PAN combined with ca. 10 wt % carbon yield from the Pluronic. Sample CCM-PCT-2 had more than twice the carbon content of CCM-PCT-1 due to the much larger PAN fraction of the block

terpolymer coupled with a similar Titania:EO molar ratio (ca. 1.55). Thus, the PAN fraction of a Pluronic-PAN block terpolymer can tune the carbon content of the final three-component nanocomposite when all other conditions are held constant.

The increased PAN fraction in the Pluronic-PAN2 used for CCM-PCT-2 also effected the resulting porosity. The nitrogen physisorption analysis of CCM-PCT-2 exhibited a type IV isotherm (Figure 3B, dashed line). Analysis of this isotherm showed a much larger total surface area of  $238 \text{ m}^2/\text{g}$  and pore volume of  $0.27 \text{ cm}^3/\text{g}$ . The mesoporous surface area of  $131 \text{ m}^2/\text{g}$  was nearly identical to that of CCM-PCT-1. The much larger microporous surface area of  $107 \text{ m}^2/\text{g}$  in CCM-PCT-2 is attributed to its larger carbon fraction. The BJH analysis on the adsorption isotherm indicated that the mesopores had a narrow distribution of pore diameters centered at 16.5 nm (Figure 3B inset, dashed line). The larger PAN fraction and PAN molecular weight of the polymer used in CCM-PCT-2 are expected to result in higher PAN crystallinity and thus cause more PEO and PPO chain stretching. The expected additional PPO chain stretching is consistent with the observed increase in mesopore diameter. The use of a block terpolymer with a larger weight fraction of PAN resulted in a nanocomposite that had more wt % carbon, larger diameter mesopores, and increased microporous surface area.

A control sample, CCM-PCT-3, was synthesized from P123 to further understand the role of PAN in the previous nanocomposites. Although others have reported nearly complete removal of Pluronic polymers under either oxidative<sup>2</sup> or inert<sup>15</sup> atmospheres, we found that the two-step heat treatment utilized here resulted in an appreciable carbon residue. Subsequent oxidative TGA of CCM-PCT-3 showed a single-step weight loss starting at  $400 \text{ }^\circ\text{C}$ , corresponding to the loss of 11.3 wt % carbon (Figure 3A, dotted line). This amount of carbon residue corresponds to a 10.7 wt % carbon yield from P123. The heat treatment to  $250 \text{ }^\circ\text{C}$  in air likely converts the Pluronic to some partially pyrolyzed products which were then more stable under the subsequent heat treatment to  $700 \text{ }^\circ\text{C}$  under  $\text{N}_2$ . TEM of CCM-PCT-3 showed that the inverse hexagonal structure present after the  $250 \text{ }^\circ\text{C}$  heat treatment collapsed during the subsequent  $700 \text{ }^\circ\text{C}$  calcination (Supporting Information, Figures S3A,B). Thus, the carbon resulting from P123 alone was insufficient to preserve the mesostructure during crystallization of the titania. In contrast, the in situ hard template resulting from PAN carbonization in CCM-PCT-1 and CCM-PCT-2 acted as a scaffold to preserve the mesostructure during the high-temperature titania crystallization. Nitrogen physisorption analysis showed that CCM-PCT-3 had a type IV isotherm with a  $\text{H}_2$  type hysteresis loop<sup>58</sup> (Figure 3B, dotted line). This hysteresis loop is indicative of ink-bottle-type pores and is due to the connected interstitial spaces of the collapsed mesostructure. BJH analysis of the adsorption branch showed a narrow mesopore diameter distribution with a maximum at 6.0 nm (Figure 3B inset, dotted line). Although the originally ordered mesostructure collapsed during calcination to form CCM-PCT-3, the final material had a powder XRD spectrum consistent with crystalline anatase titania (average domain size 10.8 nm) and a Raman spectrum consistent with partially graphitic carbon (Supporting Information Figures S3C,D). Thus, nanocomposite CCM-PCT-3 may still be of interest for electrochemical applications. The addition of PAN to Pluronic polymers was necessary to preserve the microphase-separated structure through calcination.

## Conclusions

We report the first use of a block terpolymer for the synthesis of three-component nanocomposites toward the goal of block sequence-directed materials (BSDM). Pluronic-PAN block terpolymers were synthesized from P123 and F127 macroinitiators. The resulting pentablock terpolymers were used in a simple one-pot process to produce porous nanocomposites containing tunable amounts of partially graphitic carbon and anatase titania. A sample was also made with P123 for comparison. The average mesopore diameter increased with the PAN content of the polymers. The tuning of the mesopore size is attributed to the induced PPO chain stretching due to PAN crystallization. The porosity, carbon, and titania in these nanocomposites were all controlled by varying the block ratios and molecular weights of the polymers used during self-assembly. We expect that such nanocomposites will play an increasing role in applications for energy conversion, generation, and storage.

**Acknowledgment.** This work was supported by the Cornell Fuel Cell Institute via the Cornell Center for Materials Research, a Materials Research Science and Engineering Center of the National Science Foundation (DMR-0520404). This publication was further supported by a Grant No. R21DE018335 from the National Institute of Dental and Craniofacial Research. This work made use of the Cornell Center for Materials Research Shared Facilities, supported through the NSF Materials Research Science and Engineering Centers program, and X-ray equipment supported by Department of Energy Grant DEFG-02-97ER62443.

**Supporting Information Available:** Pluronic-PAN synthesis scheme; Pluronic-PAN NMR and GPC data; SAXS of neat Pluronic-PAN1 and Pluronic-PAN2; TEM, XRD, and Raman spectrum of CCM-PCT-3; and dark field TEM of CCM-PCT-1. This material is available free of charge via the Internet at <http://pubs.acs.org>.

## References and Notes

- Warren, S. C.; Disalvo, F. J.; Wiesner, U. *Nat. Mater.* **2007**, *6* (3), 248–248.
- Zhao, D. Y.; Feng, J. L.; Huo, Q. S.; Melosh, N.; Fredrickson, G. H.; Chmelka, B. F.; Stucky, G. D. *Science* **1998**, *279* (5350), 548–552.
- Templin, M.; Franck, A.; DuChesne, A.; Leist, H.; Zhang, Y. M.; Ulrich, R.; Schadler, V.; Wiesner, U. *Science* **1997**, *278* (5344), 1795–1798.
- Yang, P. D.; Zhao, D. Y.; Margolese, D. I.; Chmelka, B. F.; Stucky, G. D. *Nature (London)* **1998**, *396* (6707), 152–155.
- Yang, P. D.; Zhao, D. Y.; Margolese, D. I.; Chmelka, B. F.; Stucky, G. D. *Chem. Mater.* **1999**, *11* (10), 2813–2826.
- Crepaldi, E. L.; Soler-Illia, G.; Grosso, D.; Cagnol, F.; Ribot, F.; Sanchez, C. *J. Am. Chem. Soc.* **2003**, *125* (32), 9770–9786.
- Choi, S. Y.; Mamak, M.; Coombs, N.; Chopra, N.; Ozin, G. A. *Adv. Funct. Mater.* **2004**, *14* (4), 335–344.
- Warren, S. C.; Messina, L. C.; Slaughter, L. S.; Kamperman, M.; Zhou, Q.; Gruner, S. M.; DiSalvo, F. J.; Wiesner, U. *Science* **2008**, *320* (5884), 1748–1752.
- Ryoo, R.; Joo, S. H.; Jun, S. *J. Phys. Chem. B* **1999**, *103* (37), 7743–7746.
- Lee, J.; Yoon, S.; Hyeon, T.; Oh, S. M.; Kim, K. B. *Chem. Commun.* **1999**, *21*, 2177–2178.
- Kim, J.; Lee, J.; Hyeon, T. *Carbon* **2004**, *42* (12–13), 2711–2719.
- Liang, C. D.; Hong, K. L.; Guiochon, G. A.; Mays, J. W.; Dai, S. *Angew. Chem., Int. Ed.* **2004**, *43* (43), 5785–5789.
- Deng, Y. H.; Yu, T.; Wan, Y.; Shi, Y. F.; Meng, Y.; Gu, D.; Zhang, L. J.; Huang, Y.; Liu, C.; Wu, X. J.; Zhao, D. Y. *J. Am. Chem. Soc.* **2007**, *129* (6), 1690–1697.
- Fan, J.; Boettcher, S. W.; Stucky, G. D. *Chem. Mater.* **2006**, *18* (26), 6391–6396.
- Liu, R. L.; Shi, Y. F.; Wan, Y.; Meng, Y.; Zhang, F. Q.; Gu, D.; Chen, Z. X.; Tu, B.; Zhao, D. Y. *J. Am. Chem. Soc.* **2006**, *128* (35), 11652–11662.
- Liu, R.; Ren, Y.; Shi, Y.; Zhang, F.; Zhang, L.; Tu, B.; Zhao, D. *Chem. Mater.* **2008**, *20* (3), 1140–1146.
- Kruk, M.; Dufour, B.; Celer, E. B.; Kowalewski, T.; Jaroniec, M.; Matyjaszewski, K. *Chem. Mater.* **2006**, *18* (6), 1417–1424.
- Stefik, M.; Lee, J.; Wiesner, U. *Chem. Commun.* **2009**, 2532–2534.
- Lee, J.; Orillall, M. C.; Warren, S. C.; Kamperman, M.; Disalvo, F. J.; Wiesner, U. *Nat. Mater.* **2008**, *7* (3), 222–228.
- Toombes, G. E. S.; Mahajan, S.; Weyland, M.; Jain, A.; Du, P.; Kamperman, M.; Gruner, S. M.; Muller, D. A.; Wiesner, U. *Macromolecules* **2008**, *41* (3), 852–859.
- Toombes, G. E. S.; Mahajan, S.; Thomas, M.; Du, P.; Tate, M. W.; Gruner, S. M.; Wiesner, U. *Chem. Mater.* **2008**, *20* (10), 3278–3287.
- Ying, J. Y.; Mehnert, C. P.; Wong, M. S. *Angew. Chem., Int. Ed.* **1999**, *38* (1–2), 56–77.
- Schuth, F.; Schmidt, W. *Adv. Mater.* **2002**, *14* (9), 629–638.
- Guo, Y. G.; Hu, J. S.; Wan, L. J. *Adv. Mater.* **2008**, *20* (23), 4384–4384.
- Bruce, P. G.; Scrosati, B.; Tarascon, J. M. *Angew. Chem., Int. Ed.* **2008**, *47* (16), 2930–2946.
- Vichi, F. M.; Tejedor-Tejedor, M. I.; Anderson, M. A. *Chem. Mater.* **2000**, *12* (6), 1762–1770.
- Colomer, M. T. *J. Solid State Electrochem.* **2006**, *10* (1), 54–59.
- O’Hayre, R.; Prinz, F. B. *J. Electrochem. Soc.* **2004**, *151* (5), A756–A762.
- Tate, M. W.; Eikenberry, E. F.; Barna, S. L.; Wall, M. E.; Lowrance, J. L.; Gruner, S. M. *J. Appl. Crystallogr.* **1995**, *28*, 196–205.
- Tsarevsky, N. V.; Sarbu, T.; Gobelt, B.; Matyjaszewski, K. *Macromolecules* **2002**, *35* (16), 6142–6148.
- Dong, W. Y.; Sun, Y. J.; Lee, C. W.; Hua, W. M.; Lu, X. C.; Shi, Y. F.; Zhang, S. C.; Chen, J. M.; Zhao, D. Y. *J. Am. Chem. Soc.* **2007**, *129*, 13894–13904.
- Donnet, J.-B.; Bansal, R. C. *Carbon Fibers*, 2nd rev ed.; Marcel Dekker: New York, 1990; p 470.
- Jo, S. M.; Paik, H. J.; Matyjaszewski, K. *Abstr. Pap. Am. Chem. Soc.* **1997**, *213*, 325–POLY.
- Matyjaszewski, K.; Jo, S. M.; Paik, H. J.; Gaynor, S. G. *Macromolecules* **1997**, *30* (20), 6398–6400.
- Matyjaszewski, K.; Jo, S. M.; Paik, H. J.; Shipp, D. A. *Macromolecules* **1999**, *32* (20), 6431–6438.
- Lazzari, M.; Chiantore, O.; Mendichi, R.; Lopez-Quintela, M. A. *Macromol. Chem. Phys.* **2005**, *206* (14), 1382–1388.
- Ilhanli, O. B.; Erdogan, T.; Tunca, U.; Hizal, G. *J. Polym. Sci., Part A: Polym. Chem.* **2006**, *44* (10), 3374–3381.
- Leiston-Belanger, J. M.; Penelle, J.; Russell, T. P. *Macromolecules* **2006**, *39* (5), 1766–1770.
- Dong, H. C.; Tang, W.; Matyjaszewski, K. *Macromolecules* **2007**, *40* (9), 2974–2977.
- Dufour, B.; Tang, C. B.; Koynov, K.; Zhang, Y.; Pakula, T.; Matyjaszewski, K. *Macromolecules* **2008**, *41* (7), 2451–2458.
- Tang, W.; Matyjaszewski, K. *Macromolecules* **2007**, *40* (6), 1858–1863.
- Tang, W.; Matyjaszewski, K. *Macromolecules* **2006**, *39* (15), 4953–4959.
- Wanka, G.; Hoffmann, H.; Ulbricht, W. *Macromolecules* **1994**, *27* (15), 4145–4159.
- Peleshanko, S.; Jeong, J.; Shevchenko, V. V.; Genson, K. L.; Pikus, Y.; Ornatska, M.; Petrash, S.; Tsukruk, V. V. *Macromolecules* **2004**, *37* (20), 7497.
- Hobson, R. J.; Windle, A. H. *Polymer* **1993**, *34* (17), 3582–3596.
- Tian, B.; Liu, X.; Solovyov, L. A.; Liu, Z.; Yang, H.; Zhang, Z.; Xie, S.; Zhang, F.; Tu, B.; Yu, C.; Terasaki, O.; Zhao, D. *J. Am. Chem. Soc.* **2003**, *126* (3), 865–875.
- Soler-Illia, G.; Sanchez, C. *New J. Chem.* **2000**, *24* (7), 493–499.
- Kowalewski, T.; Tsarevsky, N. V.; Matyjaszewski, K. *J. Am. Chem. Soc.* **2002**, *124* (36), 10632–10633.
- Tang, C. B.; Qi, K.; Wooley, K. L.; Matyjaszewski, K.; Kowalewski, T. *Angew. Chem., Int. Ed.* **2004**, *43* (21), 2783–2787.
- Ho, R. M.; Wang, T. C.; Lin, C. C.; Yu, T. L. *Macromolecules* **2007**, *40* (8), 2814–2821.
- Lazzari, M.; Scalarone, D.; Hoppe, C. E.; Vazquez-Vazquez, C.; Lopez-Quintela, M. A. *Chem. Mater.* **2007**, *19*, 5818–5820.
- Tang, C.; Dufour, B.; Kowalewski, T.; Matyjaszewski, K. *Macromolecules* **2007**, *40* (17), 6199–6205.
- Brandup, J.; Immergut, E. H.; Grulke, E. A. *Polymer Handbook*, 4th ed.; John Wiley and Sons: New York, 1999.
- Sadezky, A.; Muckenhuber, H.; Grothe, H.; Niessner, R.; Poschl, U. *Carbon* **2005**, *43* (8), 1731–1742.
- Tuinstra, F.; Koenig, J. L. *J. Chem. Phys.* **1970**, *53* (3), 1126.
- Lespade, P.; Aljishi, R.; Dresselhaus, M. S. *Carbon* **1982**, *20* (5), 427–431.
- Kamperman, M.; Fierke, M. A.; Garcia, C. B. W.; Wiesner, U. *Macromolecules* **2008**, *41* (22), 8745–8752.
- Sing, K. S. W.; Everett, D. H.; Haul, R. A. W.; Moscov, L.; Pierotti, R. A.; Rouquerol, J.; Siemieniowska, T. *Pure Appl. Chem.* **1985**, *57* (4), 603–619.